From selective dissolution to crystal chemistry of brownmillerite in sulfate resisting cement

Alexis Mériot, Marie-noëlle de Noirfontaine, Mireille Courtial, Laurent Izoret, Sandrine Tusseau-Nenez, Mélanie Labourel, sandrine Gauffinet, Frédéric Dunstetter

From selective dissolution to crystal chemistry of brownmillerite in sulfate resisting cement

Alexis Mériot[1,2], Marie-Noëlle de Noirfontaine[1], Mireille Courtial[1,3], Laurent Izoret[2], Sandrine Tusseau-Nenez[5], Mélanie Labourel[1,2], Sandrine Gauffinet[4] and Frédéric Dunstetter[1]

[1]Laboratoire des Solides Irradiés, CEA-DRF-IRAMIS, CNRS, Ecole Polytechnique, Institut Polytechnique de Paris, 91120, Palaiseau, France

[2]Syndicat Français de l'Industrie Cimentière, 7 place de la Défense, 92974, Paris-La-Défense, France

[3]Université d'Artois, 1230 Rue de l'Université, 62408, Béthune, France

[4]Laboratoire Interdisciplinaire Carnot de Bourgogne, CNRS, Université de Bourgogne Franche-Comté, 21078, Dijon, France

[5]Laboratoire de Physique de la Matière Condensée, CNRS, Ecole Polytechnique, Institut Polytechnique de Paris, 91120, Palaiseau, France

Correspondence: Marie-Noëlle de Noirfontaine

Email: marie-noelle.de-noirfontaine@polytechnique.edu

Keywords: brownmillerite, atomic structure, Portland cement, ferrites, X-ray methods, microscopy.

Abstract

The aim of this study is to extract brownmillerite from sulfate resisting Portland cement (SRPC) in order to determine its crystal chemistry and the effects of dissolution protocols. Brownmillerites (C_4AF) from four SRPC were extracted and systematically studied by X-ray diffraction (XRD), electron probe microanalysis (EPMA) and X-ray fluorescence spectroscopy.

Two extraction steps were used. The first is the SAM protocol that leaves a residue rich in ferrite, C_3A and sulfates. Precipitated hydrated sulfate minerals are also observed for clinker with high molar SO_3/Na_2O_{eq} ratio. The second, developed in this paper, uses acetic acid (AcA) to dissolve C_3A and sulfates.

The Rietveld refinements showed that all brownmillerites of this study crystallize in *Ibm2* space group. Two families of brownmillerite were identified by their aluminum content and cell parameters, related to the presence of C_3A in the clinker. EPMA indicated that ferrites from SR0 and SR3 cements have Al/Fe ratios about 0.7 and 0.8-1.0 respectively. XRD allows to predict the (Al+Mg+Si)/Fe ratio in brownmillerite in good agreement with EPMA. The SAM protocol is the best way to study crystal chemistry of brownmillerite and the AcA protocol is recommended to dissolve sulfates and C_3A for further reactivity studies.

1 | INTRODUCTION

Portland cement clinker contains four principal minerals. Large crystals of alite (C_3S_{ss})[a] and belite (C_2S_{ss}) are embedded in an interstitial phase of a mixture of tricalcium aluminate (C_3A_{ss}) and a ferrite phase also called brownmillerite approximated to C_4AF_{ss}. C_3A and C_4AF_{ss} grains, crystallizing from the melt, are submicronic-sized (depending on the cooling rate). Alite and belite are the major phases (about 65 wt.% and 15 wt.% respectively), C_3A and C_4AF_{ss} are in minor proportions (typically 7-8 wt.% each). Other minor phases can also be found in the interstitial phase: free lime, periclase, quartz, carbonates and sulfates (alkali sulfates such as arcanite K_2SO_4, aphthitalite $3K_2SO_4.Na_2SO_4$ and calcium langbeinite $K_2SO_4.2CaSO_4$).

It is known that aluminate phases, more precisely C_3A, play a key role in the resistance of cements to external sulfate attack.[1] Cement manufacturers have limited the C_3A content in cements, which led to the normalization of SR (Sulfate Resisting) cements in Europe[2] (to be compared with cements of type V described in ASTM American standard)[3]. Three classes were thus defined: SR0, SR3 and SR5 referred to 0, 3 and 5 wt.% of C_3A in the clinker respectively. However, poor performances of SR cements are sometimes observed in sulfated medium, which raises the question of whether a threshold of aluminum content in brownmillerite is responsible for those below average performances.

[a] C = CaO; S = SiO_2; A = Al_2O_3; F = Fe_2O_3 in abbreviated oxide notation; "ss" refers to solid solution

Brownmillerite is a large solid solution between C_2F and C_6A_2F, often written as $Ca_2Al_xFe_{2-x}O_5$ with $0<x<1.4$. Despite it belongs to the orthorhombic crystal structure, it is not isostructural: it crystallizes in the space group *Pnma* for $0<x<0.4\text{-}0.6$ and in the space group *Ibm2* for $0.4\text{-}0.6<x<1.4$.[4, 5, 6] The main difference between the two structures is the stacking sequences of the tetrahedral chains. The brownmillerite structure ($A_2B_2O_5 = A_2BB'O_5$) is an oxygen-deficient perovskite-like structure (ABO_3), composed of sheets of [Fe, Al]-O octahedra normal to the b axis connected to single chains of (Al, Fe)-O tetrahedra parallel to the c axis (Figure 1). For x = 1 (Al/Fe = 1), iron and aluminum occupy 76% and 24% of the octahedral sites respectively, the opposite stands for the tetrahedral sites.[4] In usual Portland cements, it is well established that brownmillerite crystallizes in space group *Ibm2*, with Al/Fe ratio between 1 to 2 approximately.[7] Only few studies have analyzed ferrite phase of sulfate resisting Portland cements (SRPC).[8, 9, 10] It is known that the ferrite phase is more iron-rich[7] but there is a lack of quantitative and recent information on these industrial ferrites.

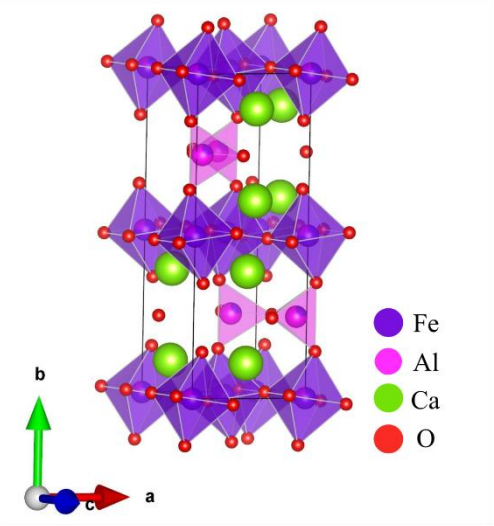

FIGURE 1 Brownmillerite crystal structure from Colville and Geller[4] (Green: calcium atom; pink: tetrahedral site; purple: octahedral site; red: oxygen atom). The graphic was drawn using the VESTA software[11]

Most of the key studies on reactivity of brownmillerite were performed on synthetic ferrites[12, 13, 14, 15, 16] which are not fully representative of the industrial phase. Indeed, industrial ferrites are different from synthetic ones, in particular by the impurities (particularly Mg and Si) incorporated from raw materials and fuels (Taylor 1997), the burning conditions (temperature and kiln atmosphere) and liquid quenching. All these parameters affect the crystal chemistry (solid solution, polymorphism), the grain size and thereby the reactivity of the material. Studying the industrial material is then the key point towards understanding and predicting its behavior in sulfated medium. Nevertheless, clinker is a multi-phase material, which leads to difficulties in studying the crystal structure of ferrite. Moreover, the ferrite crystals, with a grain size below 1 μm, are intimately intermingled with those of C_3A, hence the microstructural characterization of the ferrite from the clinker using Scanning Electron Microscopy (SEM) is not accurate enough. The usual approach[17] aimed at overpassing those technological locks is to dissolve alite, belite and free lime from the clinker using the Salicylic Acid/Methanol (SAM) quantitative selective dissolution protocol.[18] The main disadvantage of the SAM method is that C_3A and sulfate phases are not dissolved, the latter are highly reactive and can perturb the study of intrinsic reactivity of brownmillerite in sulfate medium. On the other hand, nitric acid extraction dissolves C_3A but not sulfated phases. Therefore, in order to fully extract brownmillerite from the SAM residue, a second step of dissolution was developed in this paper using acetic acid (AcA) based on the protocol proposed by Triviño.[19]

In this article, we propose a systematic study of the ferrite phase of four low C_3A content clinkers from different European plants: two without C_3A (SR0) and two with less than 3 wt.% of C_3A (SR3). These clinkers differ significantly in their mineralogical and chemical compositions, more precisely in their contents of alkali, sulfate and MgO. Clinker and residues from SAM and AcA protocols are studied by X-Ray Diffraction (XRD), XRF and Electron Probe Micro Analysis (EPMA). The advantage of EPMA over SEM is a smaller probe size and allows precise and quantitative elemental analysis by Wavelength Dispersive Spectroscopy (WDS).[20] The effects of the SAM and AcA protocols on the clinker and the ferrite will be presented. The combination of XRD, XRF and EPMA allows to precise the solid solution domain of the four ferrites.

2 | EXPERIMENTAL PROCEDURE

2.1 | Sample preparation

Four commercial clinkers (SR0 and SR3) selected from various European cement plants were provided by the Professional Syndicate of the French Cement Industry (SFIC). Fifty kilograms have been prepared using a random sampling by quartering. Two kilograms of each clinker were crushed down to less than 2.5 mm grain size with no retained grains, homogenized and then again sampled by quartering method in order to obtain 500 grams of each clinker, then ground to an average particle size of 40 µm.

A first step of selective dissolution using Salicylic Acid/Methanol extraction (SAM) was used in order to dissolve calcium silicates and free lime. This protocol is based on the NIST protocols.[18, 21] Filter funnel (porosity 4) and beaker are dried for 15 minutes at 65°C in order to avoid water. SAM solution is prepared with 70 g of salicylic acid (SaH, RP) and 400 mL of methanol (H_2O < 0.2 %). 10 g of clinker are introduced in salicylic solution with fast constant stirring for 1 hour, then the solution is vacuum filtered using the filter funnel. The beaker is recovered all the time to avoid water pollution. The residue is washed three times with 10 mL of methanol, dried during 3 h and stored in a vacuum desiccator.

A second step of selective dissolution was also performed in order to dissolve the sulfate phases and C_3A in the SAM residue. This protocol is based on the Triviño Vasquez protocol.[19] The solution is prepared with 250 mL of acetic acid 1 N, made from pure glacial acetic acid (Alfa Aesar 99+%). 2.5 g of SAM residue are stirred into this solution. After 15 minutes, the solution is filtered using a fast filtration filter (Whatman n°1). The residue is then washed with methanol and dried at 65°C for 1 hour. This protocol is hereafter referred to as the Acetic Acid (AcA) extraction.

2.2 | Analysis techniques

2.2.1 | X-ray fluorescence spectrometry

Elementary analysis of clinkers and residues (SAM and AcA) was performed by X-ray Fluorescence. Fused beads of clinkers and SAM residues were analyzed using a MAGIC X PRO spectrometer (PANalytical, Almelo, The Netherlands). AcA residues powders were analyzed using a S8 TIGER spectrometer (Bruker AXS, Karlsruhe, Germany).

2.2.2 | X-ray diffraction

XRD data of clinkers and residues (SAM and AcA) were collected using a D8 Advance powder X-ray diffractometer (Bruker AXS, Karlsruhe, Germany) in the Bragg-Brentano geometry (θ/θ). The experimental configuration was set as follows, in order to optimize the XRD signal of the calcium ferrite phase. The

incident X-ray beam (Cu radiation, 40 kV, 40 mA) passed through a fixed divergence slit of 0.4° and primary 1.6° axial Soller slits. The diffracted beam went through secondary 1.5° axial Soller slits before entering a fast 1D LynxEye XE-T of 2.915° (2θ) aperture. Soller slits with a narrow width angle are used in order to reduce the asymmetry of low angle peaks (due to the axial divergence), which is of particular importance in the case of the ferrite phase with a characteristic peak at around 12.1°. The LynxEye XE-T detector has a reduced energy discrimination window, filtering the iron fluorescence. A motorized anti-scatter screen was also used to reduce unwanted scattered radiation by the atmosphere at low angles from the main beam. The instrument was operated in step-scan mode, between 5° and 90° (2θ) with 0.005° (2θ) step and 1s per step. In order to minimized preferential orientation, the powder was prepared thanks to a backloading sample holder.

Phase identifications were performed using the DIFFRAC.EVA software (version 5, Bruker-AXS, Karlsruhe, Germany, 2010–2020). Rietveld refinements were performed using the TOPAS software (version 6, Bruker-AXS, Karlsruhe, Germany, 1999–2016) based on the fundamental parameters approach.[22] The starting structural data of the phases in clinkers and residues are listed in Table 1. The refined parameters included scale factor, sample displacement, coefficients of the background described as a fifth order Chebychev polynomial combined with a 1/X term, unit cell parameters and crystallite size (referred to as L_{vol}-IB). The atomic positions and temperature factors of all phases were kept constant in the crystal structures. Preferred orientation was corrected using March-Dollase algorithm[23] for the alite M3 60-6 and alite <M1> 300 Bragg lines. For the ferrite phase, additional refined parameters were added: a strain parameter (referred to as strain G) and the occupancy factors of aluminum and iron on tetrahedral and octahedral sites.

TABLE 1 Phases of clinkers, SAM and AcA residues: structural data, PDF and ICSD file numbers. For each phase, the ICSD codes (Inorganic Crystal Structure Database,) and PDF numbers (International Centre for Diffraction Data (ICDD) PDF,) are given for information. PDF number in parentheses corresponds to experimental data.

Phase/mineral name	Formula	Symmetry	Space group	PDF file	ICSD	Reference
M1 Alite Tricalcium silicate	Ca_3SiO_5	Monoclinic	*Pc* (7)	(00-055-0739)	—	[24]
M3 Alite Tricalcium silicate	Ca_3SiO_5	Monoclinic	*Cm* (8)	01-085-1378	64759	[25]
β-C_2S Belite (Larnite)	Ca_2SiO_4	Monoclinic	*$P2_1/n$* (14)	01-086-0398 (00-033-0302)	81096	[26]
Cubic C_3A Tricalcium aluminate	$Ca_3Al_2O_6$	Cubic	*Pa-3* (205)	01-070-0839 (00-038-1429)	1841	[27]
Ortho C_3A Tricalcium aluminate	$Ca_3Al_2O_6$	Orthorhombic	*Pbca* (61)	01-070-0859	1880	[28]
C_4AF Ferrite (Brownmillerite)	Ca_2AlFeO_5	Orthorhombic	*Ibm2* (46)	01-071-0667 (00-030-0226)	9197	[4]
Lime	CaO	Cubic	*Fm-3m* (225)	(00-037-1497)	—	[29]
Periclase	MgO	Cubic	*Fm-3m* (225)	01-071-1176 (00-045-0946)	9863	[30]
α-Quartz	α-SiO_2	Rhombohedral	*$P3_22$* (154)	(00-046-1045)	162490	[31]
Hemihydrate (Bassanite)	$CaSO_4.½H_2O$	Monoclinic	*I2* (5)	01-083-0438	79528	[32]
Arcanite	K_2SO_4	Orthorhombic	*Pnam* (62)	01-083- 0681 (00-005-0613)	79777	[33]
Aphthitalite	$K_3Na(SO_4)_2$	Trigonal	*P-3m* (164)	01-074-0398 (00-020-0928)	26018	[34]
Syngenite	$K_2Ca(SO_4)_2(H_2O)$	Monoclinic	*$P2_1/m$* (11)	01-074-1118 (00-028-0739)	26829	[35]
Ca-Langbeinite	$Ca_2K_2(SO_4)_3$	Orthorhombic	*$P2_12_12_1$* (19)	01-074-0404 (00-020-0867)	40989	[36]
Portlandite	$Ca(OH)_2$	Trigonal	*P-3m* (164)	01-084-1263 (00-004-0733)	202220	[37]

2.2.3 | Optical microscopy and electron microprobe analysis

Polished sections (2.5 cm diameter x 0.7 cm height) of clinker nodules with grain size distribution less than 10 mm and SAM residues powders were prepared by embedding the specimens in epoxy resin, followed by a fine polishing. Clinker morphology was studied under a VHX-1000 reflected light microscope (Keyence).

The elemental analysis of the ferrite phase was carried out on SAM residues using an SXFive electron microprobe analyzer (CAMECA), with operating conditions of 15 kV accelerating voltage and 4 nA beam current. This current has been chosen to reduce the interaction volume and to ensure an accurate and precise measurement of the ferrite phase composition. Prior to analysis, the polished sections were coated with a thin conductive layer (around 10 nm thick) of carbon. The chemical composition was estimated from the obtained EPMA results using the ZAF method.

3 | RESULTS AND DISCUSSION

3.1 | Clinker analyses

3.1.1 | Chemical analysis

Table 2 gives the chemical composition of the four clinkers obtained by X-Ray Fluorescence, together with the loss of ignition (LOI) and free lime (ethylene glycol test) of each sample. Their chemical compositions are very different. Clinkers A and C have an A/F ratio lower than 0.64 (0.56 and 0.58 respectively), that is the condition to avoid the formation of C_3A. Clinkers A and C are of SR0 type, the clinkers B and D of SR3 type according to the standard NF EN 197-1 2012.[2] Clinker A has the highest SO_3 to alkali ratio and clinker B has the highest MgO content.

TABLE 2 Chemical composition of the four clinkers, SAM and AcA residues (XRF, wt.%). Free CaO content was determined with the ethylene-glycol method.[7]

Oxides (wt.%)	A (SR0)			B (SR3)			C (SR0)			D (SR3)		
	Clinker	**SAM**	**AcA**	**Clinker**	**SAM**	**AcA**	**Clinker**	**SAM**	**AcA**	**Clinker**	**SAM**	**AcA**
SiO_2	21.44	2.68	2.94	20.06	3.97	3.62	21.99	3.73	3.76	21.55	3.35	3.11
Al_2O_3	3.42	12.71	13.45	4.11	15.64	15.02	2.9	14.19	13.56	3.75	16.9	15.17
Fe_2O_3	6.07	26.61	32.75	6.34	23.77	28.33	5.04	26.91	32.33	5.01	24.63	29.96
CaO	64.78	43.28	46.96	63.51	41.09	43.21	65.86	42.94	46.32	66.26	45.67	48.27
MgO	0.77	1.82	1.76	3.49	10.97	7.96	1.19	3.28	2.37	0.66	1.78	1.87
MnO	0.07	0.25	0.34	0.07	0.19	0.24	0.08	0.32	0.41	0.07	0.27	0.36
SO_3	1.54	8.1	0.84	0.45	1.44	0.13	0.55	3.85	0.13	0.49	2.95	0.08
K_2O	0.55	1.88	0.03	0.47	0.77	0.06	0.63	2.25	0.12	0.55	1.76	0.05
Na_2O	0.08	0.14	—	0.3	0.49	0.14	0.22	0.51	0.07	0.11	0.2	—
SrO	0.09	0.11	0.07	0.13	0.13	0.12	0.03	0.03	0.03	0.03	0.04	0.03
P_2O_5	0.18	0.22	0.02	0.11	0.05	—	0.08	0.09	—	0.33	0.2	0.03
TiO_2	0.18	0.44	0.58	0.26	0.69	0.86	0.15	0.4	0.51	0.23	0.6	0.78
LOI	0.42	2.00	—	0.19	0.78	—	0.51	1.07	—	0.31	0.88	—
Total	99.59	100.24	99.74	99.49	99.98	99.69	99.23	99.57	99.61	99.35	99.23	99.71
Al_2O_3/Fe_2O_3 (A/F modulus)	0.56	0.48	0.41	0.65	0.66	0.53	0.58	0.53	0.42	0.75	0.69	0.51
Na_2O_{eq} (*)	0.44	1.38	0.02	0.61	1.00	0.18	0.63	1.99	0.15	0.47	1.36	0.03
SO_3/Na_2O_{eq}	3.48	5.88	42.55	0.74	1.44	0.72	0.87	1.93	0.87	1.04	2.17	2.43
SO_3/Na_2O_{eq} (mol)	2.72	4.59	33.23	0.58	1.13	0.57	0.68	1.51	0.68	0.81	1.70	1.90
Free CaO	1.00	—	—	1.63	—	—	2.86	—	—	1.16	—	—

(*) $Na_2O_{eq} = Na_2O + 0.658\ K_2O$

3.1.2 | Mineralogical analysis

Optical microscopy of the four clinkers is sketched in Figure 2. Large crystals of alite (polygonal-shaped) and belite (rounded-shaped) are embedded in an interstitial phase where ferrite is the major phase (bright level). In this interstitial phase, only ferrite (bright) is visible for the SR0 clinkers (A and C), whereas darker small crystals of C_3A are observed in the ferrite phase for the SR3 clinkers (B and D).

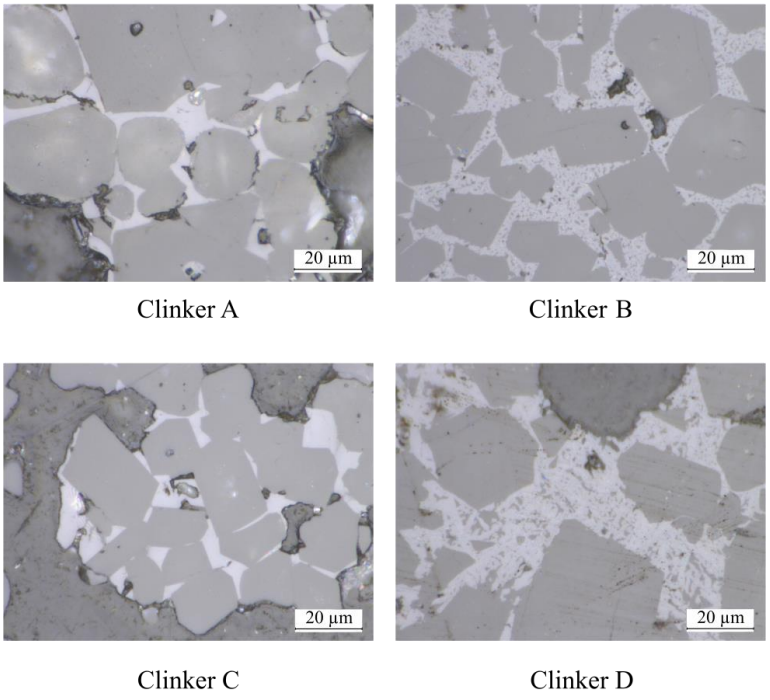

FIGURE 2 Polished section of the four cement clinkers. Interstitial phase: Ferrite phase: (bright); aluminate phase (grey). Other areas: alite, belite, porosity

The identified phases in the clinkers by XRD are (i) alite (M1 or M3 polymorphs),[24] belite (polymorph β), ferrite and (ii) in minor proportions, CaO free lime, C_3A for clinkers B and D (orthorhombic & cubic polymorphs referred to as C_3Ao and C_3Ac in the following), MgO (periclase) for clinker B, α-quartz for clinker C and arcanite for clinker D. The Rietveld quantitative analysis of the clinkers (Table 3) confirms the absence of C_3A in the SR0 clinkers (A and C), and a content of C_3A less than 3 wt.% in the SR3 clinkers (B and D). The orthorhombic polymorph of C_3A is preponderant in clinker B, as it is usually found for clinkers rich in Na_2O.[7] Periclase is found in clinker B in agreement with its high MgO content (Table 2).

TABLE 3 Phase composition (wt.%) for the four clinkers, deduced from Rietveld analysis. The ratios of C_4AF_{ss} to C_3A and C_3A cubic (C_3Ac) to orthorhombic (C_3Ao) are also written.

	A (SR0)			B (SR3)			C (SR0)			D (SR3)		
Phases	**Clinker**	**SAM**	**AcA**	**Clinker**	**SAM**	**AcA**	**Clinker**	**SAM**	**AcA**	**Clinker**	**SAM**	**AcA**
Alite M1	61.9	—	—	—	—	—	—	—	—	69.9	—	—
Alite M3		—	—	68.4	—	—	61.8	—	—	—	—	—
β-C_2S	21.8	—	—	7.7	—	—	22.6	—	—	12.8	—	—
C_3Ac	—	—	—	0.9	2.8	—	—	—	—	1.6	6.4	—
C_3Ao	—	—	—	1.2	5.7	—	—	—	—	0.3	4.7	—
C_4AF_{ss}	16.2	86.8	99.4	17.6	77.2	90.0	13.3	92.8	98.9	14.4	84.7	99.7
Lime	0.1	—	—	1.1	—	—	2.2	—	—	0.3	—	—
Periclase	—	—	—	3.1	14.2	9.8	—	1.3	0.3	—	—	—
Quartz	—	0.1	0.6	—	0.1	0.2	0.1	0.4	0.6	—	0.3	0.3
Arcanite	—	—	—	—	—	—	—	1.5	—	0.7	2.9	—
Syngenite	n.d.	5	—	—	—	—	—	—	—	—	—	—
Aphthitalite	—	—	—	—	—	—	—	4.0	—	—	1.0	—
Ca-Langbeinite	—	1.1	—	—	—	—	—	—	—	—	—	—
Hemi-hydrate (Bassanite)	—	7	—	—	—	—	—	—	—	—	—	—
Portlandite	—	—	—	—	—	—	—	—	0.2	—	—	—
Total	100	100	100	100	100	100	100	100	100	100	100	100
C_4AF_{ss}/C_3A	—	—	—	8.4	9.1	—	—	—	—	7.6	7.6	—
C_3Ac/C_3Ao	—	—	—	0.8	0.5	—	—	—	—	5.3	1.4	—

3.2 | Insoluble residue analyses

3.2.1 | After SAM treatment

The elementary and mineralogical compositions of SAM residues are given in Tables 2 and 3 respectively. Figure 3A shows the effect of the SAM protocol on XRD patterns, for example in clinker A. Alite, belite and free lime are totally dissolved. The efficiency of the SAM extractions is given in Table 4. The mass difference between the sum of the phases (alite+belite+free CaO) in clinker estimated via XRD Rietveld analysis and the mass dissolved by SAM extraction is small. This confirms that the protocol is quantitative for all the clinkers and that no other phase is dissolved by the SAM protocol.

Silicate phases are not pure phases but are solid solutions[7] and contain in particular aluminum and iron as impurities. During the dissolution, these impurities are released which explains the difference of the A/F ratio between clinker and SAM (Table 2). The red color of the SAM solution is consistent with the presence of iron in the silicate phases. The SiO_2 content remaining in the SAM residue (Table 2) can be explained by the fact that silicon is either a quartz component and an impurity in the ferrite.[7, 17, 38]

As a general rule, the SAM protocol reveals minor phases, not detected in the clinker, and allows a better identification and quantification of C_3A polymorphs. For clinkers A, B and D, it reveals the presence of a small amount of quartz. The presence of the orthorhombic C_3A polymorph is highlighted in SAM residue of clinker D (Figure 3B). As it is difficult to determine the precise amount of C_3A in SRPC via XRD and XRF, the SAM protocol was proposed to allow a better quantification.[39] In the present samples, the C_4AF_{ss}/C_3A ratios calculated from the Rietveld refinements of the clinkers and the SAM residues are very similar. However, the C_3Ac/C_3Ao ratio is not constant, especially in clinker D where it is 4 times superior to the SAM residue (Table 3). Rietveld analysis of the clinker underestimates the amount of C_3Ao. Therefore, a SAM dissolution is needed in order to measure the correct balance of C_3A polymorphs, as was also found by Le Saoût et al.[17] for other types of Portland cement. Minor contents of periclase MgO, aphthitalite and arcanite are highlighted in SAM of clinker C, whereas calcium langbeinite is found in SAM of clinker A.

As can be seen in Figure 3A in the specific case of clinker A, the XRD Bragg lines of alite and belite disappear in the SAM residue, whereas broad lines of the hemi-hydrate and syngenite sulfate phases, now appear. The presence of hemi-hydrate in the SAM residue was also confirmed by TGA. The presence of a very small proportion of syngenite in clinker A cannot be totally excluded. The Rietveld refinement of the SAM residue gave about 13 wt.% of these crystalline sulfate phases (syngenite and hemi-hydrate). The sulfate content is not affected at all by the protocol, and one observes the same amount of sulfate in the clinker and in the SAM residue for all clinkers, weighted by the yield (Tables 2 and 4). However, clinker A is very different from the three other clinkers in what concerns its very high molar SO_3

to alkali ratio $(SO_3/Na_2O_{eq})_{mol}$ also called "sulfatisation degree" (2.72 compared to 0.58; 0.68; 0.81 for clinkers B, C and D respectively). As shown by [7, 40, 41], SO_3 and alkali are then incorporated in belite and alite. Therefore, our hypothesis is that alkalis and SO_3 of silicate phases in clinker A were released during the SAM extraction and precipitated in hydrated sulfate minerals (syngenite and bassanite). Several trials performed in five laboratories also showed the presence of these sulfate phases in clinker A, with small variations in nature and proportion probably due to experimental conditions (temperature and humidity).

TABLE 4 Efficiency (wt.%) of the SAM and AcA extractions

Method		**Clinker A**	**Clinker B**	**Clinker C**	**Clinker D**
SAM	Average extraction yield (a minimum of 20 samples per clinker)	19 (1)	23 (2)	16 (1)	17 (1)
	(1) XRD: Alite+Belite+CaO in clinker	83.8	77.2	86.6	83
	(2) SAM: total dissolved	81	77	84	83
	Difference (1) - (2)	2.8	0.2	2.6	0
AcA	Extraction yield	64	68	62	54
	(3) XRD: C_3A+sulfate phases in SAM residue	13.1	8.5	5.5	15
	(4) AcA: total dissolved	36	32	38	46
	Difference (3) - (4)	-22.9	-23.5	-32.5	-31

(A) (B)

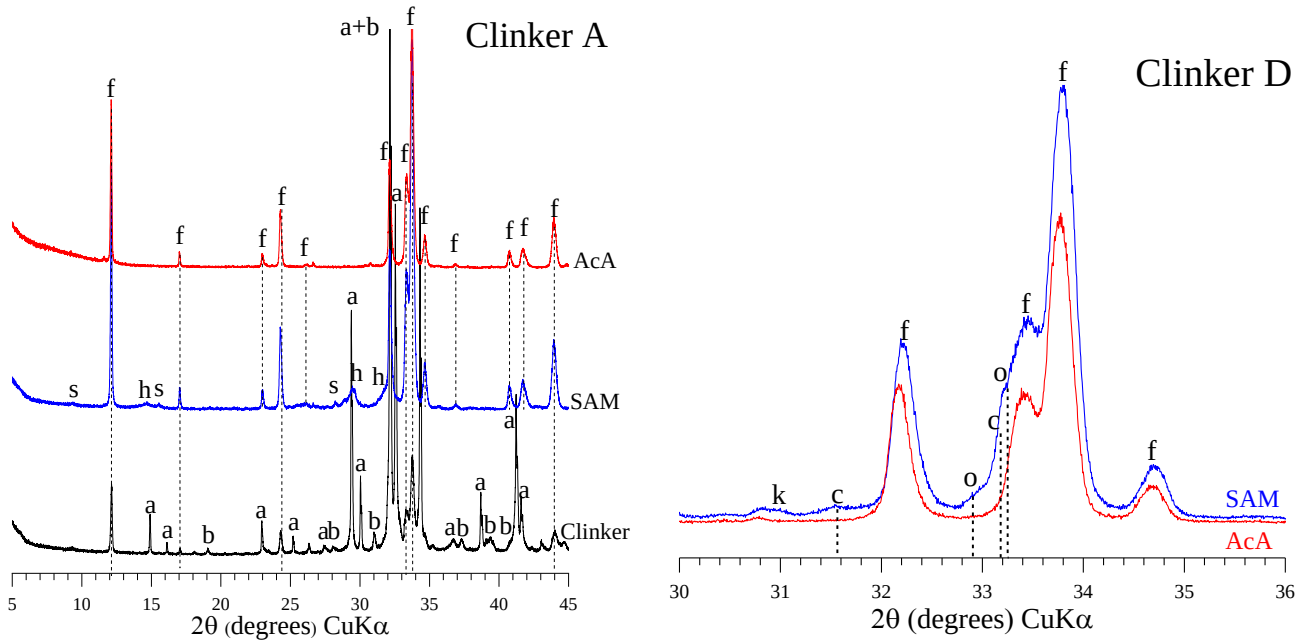

FIGURE 3 (A) XRD patterns of clinker, SAM and AcA residues of clinker A (B) XRD patterns of SAM and AcA residues of clinker D (a: alite; b: belite; f: ferrite; h: hemi-hydrate; s: syngenite; c: cubic C_3A; o: orthorhombic C_3A; k: arcanite)

3.2.2 | After acid acetic (AcA) extraction

Acetic acid is used to dissolve the sulfate and C_3A phases of the SAM residue. This protocol appears to be very effective. As shown by XRD (Figure 3 and 4), the sulfate and C_3A phases disappear and the periclase content decreases. No hydrate is observed.

However, a drawback of the method arises due to the presence of water, which reduces the remaining ferrite amount. The difference between the mass of phases supposed to be dissolved (C_3A + sulfate) and the real amount dissolved supposes that ferrite is partially dissolved (Tables 3 and 4). Roughly one third of the ferrite of the SAM residue is dissolved. For all clinkers, the XRD refinements exhibit larger crystallites for the AcA residue than for the SAM residue (Table 5), which is consistent with the dissolution of the smallest grains of ferrite.

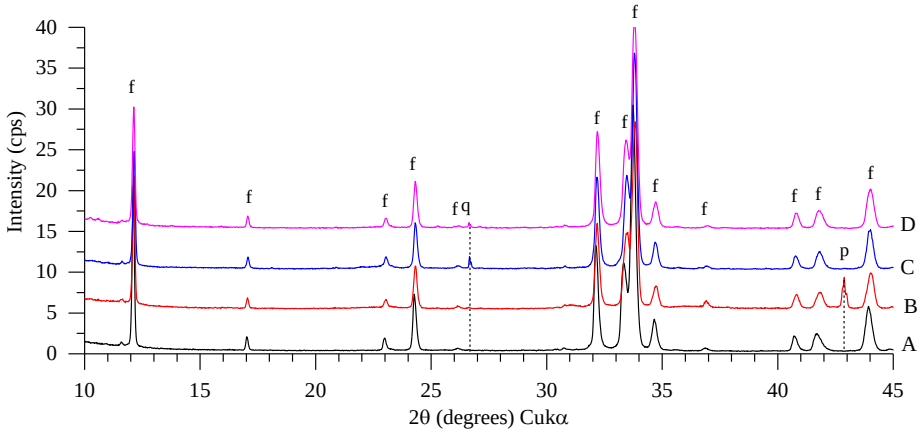

FIGURE 4 XRD patterns of the four AcA residues (f: ferrite, q: quartz, p: periclase)

3.3 | Ferrite crystal chemistry

3.3.1 | Crystal structure parameters from XRD/Rietveld analysis

Colville and Geller[4] gave the following cell parameters of a brownmillerite Al/Fe = 1: a = 5.584 Å, b = 14.6 Å, c = 5.374 Å, with the cationic distribution $Ca_2[Fe_{0.76}Al_{0.24}](Fe_{0.24}Al_{0.76})O_5$, in this formula the occupancy of the octahedral site is represented by [] and the occupancy of the tetrahedral site by ().

Since the ferrite of SRPC is richer in iron than the ferrite from ordinary Portland cement (OPC), the question of the relevant space group of brownmillerite, *Ibm2* or *Pnma*, is raised. The Bragg reflection 131 (29.2° 2θ Cukα) is characteristic of *Pnma* space group and can be used to detect the *Pnma* to *Ibm2* phase transition.[42] For our four clinkers, this reflection was never detected in the extracted ferrites. As for OPC cements, the ferrite phase of SPRC studied here crystallizes in the *Ibm2* space group. However, some intensities are not well reproduced by the Rietveld refinement. In particular, the observed Bragg reflections 121 (26° 2θ Cukα) and 211 (36.9° 2θ Cukα) are always lower than the calculated lines (Figure 5). The same difference was observed by Gollop and Taylor for the same 121 Bragg reflection.[9]

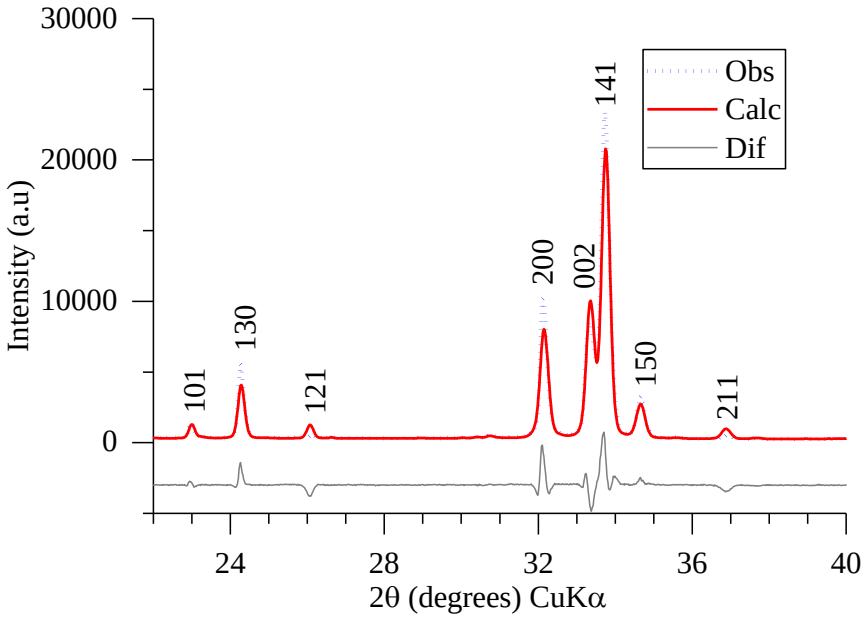

FIGURE 5 Rietveld refinement profile for XRD data of the AcA residue A: observed, calculated and difference patterns

The refined parameters of the ferrite phase in the clinkers, SAM residue and AcA residue are given in Table 5. For a same clinker, the refined lattice parameters are very similar, which proves that the selective dissolutions have no effect on the cell parameters.

Considering their cell volumes, two families of ferrite can be defined (Figure 6A): one family A&C with a cell volume between 435.79Å^3 and 436.87Å^3, and a second one B&D with a cell volume between 434.29Å^3 and 434.86Å^3. These families correspond to the two types of SRPC, SR0 and SR3. The higher cell volume for the family A&C can be explained by the higher iron content in the ferrite. As the ionic radius of Fe^{3+} is greater than that of Al^{+3} (0.645Å *vs* 0.535Å in octahedral coordination and 0.49Å *vs* 0.39Å in tetrahedral coordination),[43] the cell volume increases with to the iron content.

Figure 6B shows the Al/Fe ratio deduced from refinement site occupancies for each SAM and AcA residue. The values are not reported for the clinkers since there are meaningless, as previously pointed out by Le Saoût et al.[17]: refining such occupancies in a minor phase gives unreliable values.

The Al/Fe atomic ratios on SAM and AcA are found higher in the A&C family, which is consistent once again with the higher iron content for A&C than for B&D. The position and intensity of the 020 reflection (12° 2θ Cukα) are very sensitive to the distribution and amount of aluminum and iron in the ferrite,[44, 45] which is not observed here. This indicator can no longer be used alone in such a narrow range of composition of these four ferrites.

TABLE 5 Brownmillerite crystal structure parameters from Rietveld analyses of clinkers A-D, SAM and AcA residues: unit cell parameters, Al/Fe ratio, crystallite size L_{vol}-IB and strain parameter ε_0, together with criteria of fit (weighted-profile R_{wp} factor and R_{Bragg} factor). In parenthesis, estimated standard deviations values calculated by TOPAS.

		A (SR0)	B (SR3)	C (SR0)	D (SR3)
a (Å)	Clinker	5.5667 (5)	5.5607 (5)	5.5597 (6)	5.5550 (6)
	SAM	5.5666 (1)	5.5603 (1)	5.5630 (1)	5.5550 (1)
	AcA	5.5673 (1)	5.5606 (1)	5.5659 (1)	5.5580 (1)
b (Å)	Clinker	14.6068 (7)	14.6003 (8)	14.6299 (10)	14.6046 (9)
	SAM	14.6126 (4)	14.5859 (3)	14.6172 (4)	14.6042 (4)
	AcA	14.6112 (4)	14.5846 (3)	14.6111 (3)	14.5971 (4)
c (Å)	Clinker	5.3687 (3)	5.3550 (4)	5.3619 (5)	5.3601 (5)
	SAM	5.3704 (1)	5.3549 (1)	5.3615 (1)	5.3573 (1)
	AcA	5.3705 (1)	5.3558 (1)	5.3608 (1)	5.3590 (1)
Volume ($Å^3$)	Clinker	436.54 (5)	434.76 (6)	436.12 (7)	434.86 (7)
	SAM	436.84 (2)	434.29 (2)	435.98 (2)	434.61 (2)
	AcA	436.86 (2)	434.35 (1)	435.96 (2)	434.78 (2)
Al/Fe	Clinker	0.60 (4)	1.01 (6)	0.53 (4)	0.66 (4)
	SAM	0.93 (2)	1.08 (2)	0.96 (2)	1.11 (2)
	AcA	0.85 (2)	1.14 (2)	0.92 (2)	1.13 (2)
Crystallite size – L_{vol}-IB (nm)	Clinker	150 (10)	120 (7)	70 (3)	96 (5)
	SAM	98 (2)	113 (2)	73 (1)	88 (1)
	AcA	143 (3)	173 (4)	111 (2)	108 (2)
Strain ε_0 (%)	Clinker	0.172 (2)	0.159 (2)	0.174 (3)	0.183 (2)
	SAM	0.159 (1)	0.153 (1)	0.150 (1)	0.163 (1)
	AcA	0.146 (1)	0.145 (1)	0.136 (1)	0.143 (1)
R_{Bragg}	Clinker	4.9	4.5	3.9	3.7
	SAM	5.8	4.0	5.0	4.5
	AcA	7.0	4.3	5.5	5.7
R_{wp}	Clinker	13.7	15.3	12.8	12.2
	SAM	15.3	12.3	14.1	12.6
	AcA	15.3	13.2	14.4	14.8

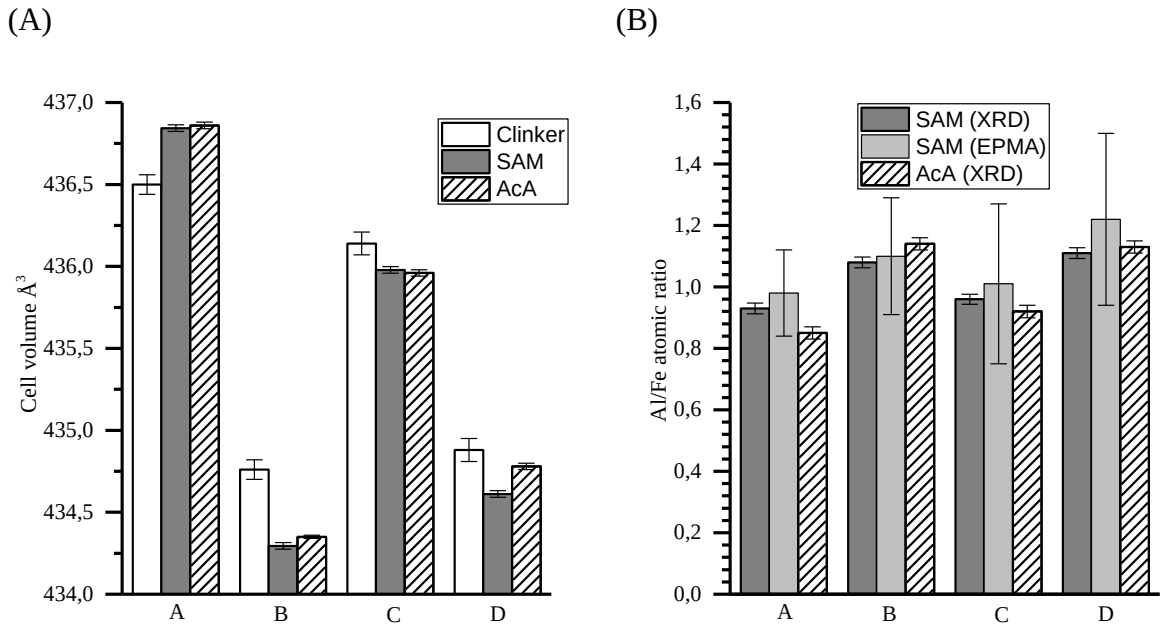

FIGURE 6 (A) Brownmillerite unit cell volume in the four clinkers (A, B, C and D), SAM and AcA residues (B) Al_{eq}/Fe atomic ratio calculated from XRD analysis of SAM and AcA residues and from EPMA measurements on SAM residues, adding Si and Mg with Al contents as explained in the text (section 3.3.2)

3.3.2 | Chemistry from EPMA and XRD

The major difficulty in XRD is the impossibility to distinguish the contribution of Al, Mg and Si atoms due to their very similar atomic scattering factors.[46] With respect to their atomic factors, the contributions of Al, Mg and Si are averaged by the diffraction technique and these atoms are "seen" as an averaged equivalent atom, referred to as Al_{eq} in the following. Therefore, the so-called Al/Fe atomic ratio refined by XRD represents a Al_{eq}/Fe ratio,[17] which precludes to determine the actual composition with XRD alone. Additional results are then needed to separate the Al, Mg and Si atoms. The EPMA analysis allows to distinguish between the atoms.

As can be seen in Table 2, the A/F value of the AcA residue is lower than the value observed in the SAM residue, which is not expected for the A and C clinkers which exhibit no aluminate in their SAM residue. A fraction of aluminum of ferrite appears to be lost during the AcA extraction. This is consistent with a loss of about 30 wt.% of the ferrite phase during the AcA dissolution. This renders the SAM residue more representative of the chemistry of the initial ferrite with respect to a quantitative measurement. Structural formulas of ferrite normalized to five oxygen atoms are then determined starting from the EPMA measurements of the SAM residues (Table 6).

In each brownmillerite, the measurements show a slightly higher calcium stoichiometry compared to the classic formula and the contents of Mg^{2+} and Si^{4+} are similar, which ensures the electrical neutrality of the crystal. Other impurities such as Ti, K, Mn and Na were detected in very small amount, with a factor of ten weaker than Si and Mg contents. Due to these impurities, the formula $Ca_2Al_xFe_{2-x}O_5$ ought to be replaced by $Ca_vMg_wAl_xFe_ySi_zO_5$.

These structural formulas are similar to those found in the literature for sulfate resisting cements [8, 9, 10, 17, 47, 48, 49, 50] and oil well cements.[51, 52, 53] The microprobe results show that brownmillerite is highly inhomogeneous, with some areas very rich in Al. This was also reported by Landa-Canova et al.[8] and Richardson et al.[53] using transmission electron microscope. Ball et al.[54] showed an Al enriched composition at the surface of ferrite grains.

EPMA then allows to obtain either the correct Al/Fe atomic ratio or the (Al+Mg+Si)/Fe atomic ratio (Table 6 and Figure 6B). The (Al+Mg+Si)/Fe atomic ratio measured by EMPA is very close to the Al_{eq}/Fe atomic ratio refined by XRD. The agreement between the two methods shows that XRD is a good tool to predict the (Al+Mg+Si)/Fe atomic ratio in ferrite. Despite the drawbacks of XRD with respect to a proper Al/Fe ratio, previously described, we obtain rather good results with XRD, which is much easier experimental method in an industrial environment. The results of Table 6 show that XRD slightly underestimates the ratio.

TABLE 6 Average ferrite formula from selected electron micro-probe data on the SAM residue compared to XRD. *number of selected analyses for each clinker. (standard deviations in parentheses)

Clinker	**Structural formula**	**Al/Fe**	**(Al+Mg+Si) /Fe**	**Al_{eq}/Fe**
Method	**EPMA**	**EPMA**	**EPMA**	**XRD**
C_4AF_{ss}	$Ca_2Al_xFe_{2-x}O_5$	x/(2-x)		x/(2-x)
A 5*	$Ca_{2.08(4)}Mg_{0.13(1)}Al_{0.69(8)}Fe_{0.98(8)}Si_{0.14(5)}O_5$	0.71 (11)	0.98 (14)	0.93
B 5*	$Ca_{2.05(4)}Mg_{0.10(2)}Al_{0.80(16)}Fe_{0.94(7)}Si_{0.11(5)}O_5$	0.87 (24)	1.10 (19)	1.08
C 6*	$Ca_{2.11(8)}Mg_{0.16(5)}Al_{0.67(7)}Fe_{0.98(12)}Si_{0.13(6)}O_5$	0.69 (12)	1.01 (26)	0.96
D 7*	$Ca_{2.12(3)}Mg_{0.11(1)}Al_{0.80(9)}Fe_{0.87(12)}Si_{0.13(3)}O_5$	0.95 (23)	1.22 (28)	1.11

Finally, the range of Al/Fe ratio of the four SRPC is shown in Figure 7, in comparison with other SR cements and OPC.

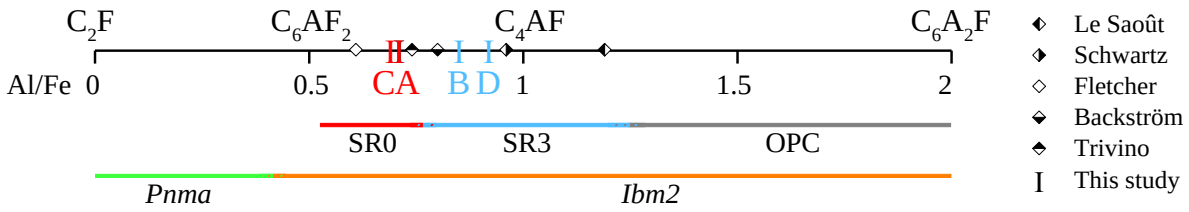

FIGURE 7 Ferrite solid solution for SR clinkers (this study and literature[10, 17, 19, 47, 48]) as a function of Al/Fe ratio

4 | CONCLUSION

In this paper, the brownmillerites of four low C_3A clinkers (two SR0 and two SR3 clinkers) were extracted by selective dissolutions in order to study their crystal chemistry. Two dissolution steps were applied: the first step is the classical "SAM" method in order to dissolve calcium silicates and free lime, followed by a second step with acetic acid (referred to as "AcA" method), seldom reported in the literature, aims at dissolving C_3A and sulfate phases.

The SAM protocol dissolves efficiently C_3S, C_2S and free lime. This protocol is quantitative and allows a better phase identification by XRD. However, sulfate and alkali contents are not affected by the protocol and it is supposed that they precipitate under the form of hydrated sulfate minerals during the SAM dissolution for clinkers with high molar SO_3/Na_2O_{eq} ratio. The protocol by acetic acid dissolves all the C_3A and sulfate phases, but it also dissolves about 30 wt.% of the ferrite phase, which makes it suitable for reactivity measurements but not appropriate for ferrite structural characterization.

The crystal chemistry of brownmillerites, including unit cell parameters and Al/Fe ratio determinations, was deduced from XRD Rietveld analysis of the residues. For all clinkers, the ferrite phase crystallizes in *Ibm2* space group. The unit cell parameters of ferrites can be correctly deduced from Rietveld analysis of both XRD patterns of clinkers and residues. The structural formulas were determined in the SAM residues using EPMA measurements. There is a good agreement between the (Al+Mg+Si)/Fe ratios evaluated by XRD and measured by EPMA. Besides, Al/Fe ranges between 0.7 and 0.9 versus 1-2 in more common Portland cements. Two families of ferrite are clearly identified: the family Al/Fe ≈ 0.7 and the family Al/Fe ≈ 0.8-0.9 for ferrites extracted from SR0 and SR3 clinkers respectively. These two families

are also highlighted by XRD. SR0 clinker ferrites exhibit larger unit cell volumes than SR3 ones, which is consistent with a stronger Al insertion in ferrites in SR3 clinkers.

Further spectroscopy measurements (Mössbauer, Raman) are in progress in order to get more information about the distribution of iron and aluminum between octahedral and tetrahedral sites, together with reactivity experiments to correlate crystal chemistry with reactivity of calcium ferrites from SR clinkers.

ACKNOWLEDGMENTS

This work was supported by SFIC (Syndicat Français de l'Industrie Cimentière) and ANRT (Association Nationale de la Recherche et de la Technologie), under the CIFRE contract 2019/0803. The authors acknowledge the support of the X-ray crystallography facility, DIFFRAX, in Ecole polytechnique, Institut Polytechnique de Paris. Michel Fialin and Nicolas Rividi are thanked for their assistance during EMPA analyses at the CAMPARIS facility in Paris. The authors thank Alexandre Tanguy (LMS, Ecole polytechnique, Institut Polytechnique de Paris) for his help for optical microscopic observation, Heloïse Reynaud and Agnes Eyraud for the preparation of polished sections (Vicat company, France).

References

1. T. Thorvaldson, "Chemical aspects of the durability of cement products," pp. 437-67 in 3th International Symposium on the Chemistry of Cement. London, UK; (1952). p. 137-67.
2. AFNOR Association Française de Normalisation, "Ciments. Partie 1 Composition, spécifications et critères de conformité des ciments courants," NF EN 197-1 (2012).
3. ASTM International, "Standard Specification for Portland Cement," ASTM C 150-07 (2007).
4. A. A. Colville and S. Geller, "The crystal structure of brownmillerite, Ca_2FeAlO_5," *Acta Crystallographica B*, 27 2311-15 (1971).
5. A. A. Colville and S. Geller, "The crystal structure of $Ca_2Fe_{1.43}Al_{0.57}O_5$ and $Ca_2Fe_{1.28}Al_{0.72}O_5$," *Acta Crystallographica B*, 28 3196-200 (1972).
6. G. Redhammer, G. Tippelt, G. Roth, and G. Amthauer, "Structural variations in the brownmillerite series $Ca_2(Fe_{2-x}Al_x)O_5$: single-crystal X-ray diffraction at 25°C and high-temperature X-ray powder diffraction (25 °C ≤ T ≤ 1000 °C)," *American Mineralogist*, 89 405–20 (2004).
7. H. F. W. Taylor, "Cement Chemistry." 2nd edition, Thomas Telford Edition: London, (1997).

8. A. R. Landa-Canova and S. Hansen, "Transmission electron microscopic study of ferrite in sulfate-resisting Portland cement clinker," *Cement and Concrete Research,* 29 679-86 (1999).
9. R. S. Gollop and H. F. W. Taylor, "Microstructural and microanalytical studies of sulfate attack. II. Sulfate resisting Portland cement: ferrite composition and hydration chemistry," *Cement and Concrete Research,* 24[7] 1347-58 (1994).
10. E. Backström and S. Hansen, "X-ray mapping of interstitial phases in sulphate resisting cement clinker," *Physical Review B,* 9[33] 17-23 (1997).
11. K. Momma and F. Izumi, "VESTA 3 for three-dimensional visualization of crystal, volumetric and morphology data," *Journal of Applied Crystallography,* 44 1272-76 (2011).
12. X. Huang, F. Wang, S. Hu, Y. Lu, M. Rao, and Y. Mu, "Brownmillerite hydration in the presence of gypsum: the effect of Al/Fe ratio and sulphate ions," *Journal of the American Ceramic Society,* 102 5545-54 (2019).
13. E. T. Carlson, "Some properties of the calcium aluminoferrite hydrates," *Journal of Research of the National Bureau of Standards,* Building Science Series 6 01-11 (1966).
14. D. Wan, W. Zhang, Y. Tao, Z. Wan, F. Wang, S. Hu, and Y. He, "The impact of Fe dosage on the ettringite formation during high ferrite cement hydration," *Journal of American Ceramic Society,* 104 3652-64 (2021).
15. N. Meller, C. Hall, A. C. Jupe, S. L. Colston, S. D. M. Jacques, P. Barnes, and J. Phipps, "The paste hydration of brownmillerite with and without gypsum: a time resolved synchrotron diffraction study at 30, 70, 100 and 150 °C," *Journal of Materials Chemistry,* 14 428-35 (2004).
16. Y. Tao, D. Wan, W. Zhang, F. Wang, and S. Hu, "Intrinsic reactivity and dissolution characteristics of tetracalcium aluminoferrite," *Cement and Concrete Research,* 146 106485 (2021).
17. G. Le Saoût, V. Kocaba, and K. Scrivener, "Application of the Rietveld method to the analysis of anhydrous cement," *Cement and Concrete Research,* 41 133-48 (2011).
18. P. E. Stutzman, P. Feng, and J. W. Bullard, "Phase analysis of Portland cement by combined quantitative X-Ray powder diffraction and scanning electron microscopy," *Journal of Research of the National Institute of Standards and Technology,* 121 47-107 (2016).
19. F. Triviño Vazquez, "Aplicaciones del metodo de Takashima, al estudio y separacion de las fases aluminoferriticas del clinker," *Materiales de Construccion,* 21[143] 21-24 (1971).
20. D. Mori and K. Yamada, "A review of recent applications of EPMA to evaluate the durability of concrete," *Journal of Advanced Concrete Technology,* 5[3] 285-98 (2007).
21. W. A. Gutteridge, "On the dissolution of the interstitial phases in Portland cement," *Cement and Concrete Research,* 9[3] 319-24 (1979).

22. R. W. Cheary and A. A. Coelho, "A fundamental parameters approach to X-ray line-profile fitting," *Journal of Applied Crystallography,* 25[2] 109-21 (1992).

23. W. A. Dollase, "Correction of intensities for preferred orientation in powder diffractometry: application of the March Model," *Journal of Applied Crystallography,* 19[4] 267-72 (1986).

24. M.-N. de Noirfontaine, F. Dunstetter, M. Courtial, G. Gasecki, and M. Signes-Frehel, "Polymorphism of tricalcium silicate, the major compound of Portland cement clinker: 2. Modelling alite for Rietveld analysis, an industrial challenge," *Cement and Concrete Research,* 36[1] 54-64 (2006).

25. F. Nishi and Y. Takéuchi, "Tricalcium silicate $Ca_3O[SiO_4]$: the monoclinic superstructure," *Zeitschrift für Kristallographie,* 172 297-314 (1985).

26. W. Mumme, L. M. D. Cranswick, and B. Chakoumanos, "Rietveld crystal structure refinements from high temperature neutron powder diffraction data for the polymorphs of dicalcium silicate," *Neues Jahrbuch für Mineralogie. Abhandlungen,* 170[2] 171-88 (1996).

27. P. Mondal and J. W. Jeffery, "The crystal structure of tricalcium aluminate, $Ca_3Al_2O_6$," *Acta Crystallographica B,* 31 689-96 (1975).

28. F. Nishi and Y. Takéuchi, "The Al_6O_{18} rings of tetrahedra in the structure of $Ca_{8.5}NaAl_6O_{18}$," *Acta Crystallographica B,* 31 1169-73 (1975).

29. H. F. McMurdie, M. C. Morris, E. H. Evans, B. Paretzkin, W. Wong-Ng, and C. R. Hubbard, "Standard X-Ray Diffraction Powder Patterns from The JCPDS Research Associateship," *Powder Diffraction,* 1[3] 265-75 (1986).

30. S. Sasaki, K. Fujino, and Y. Takéuchi, "X-ray determination of electron-density distributions in oxides, MgO, MnO, CoO, and NiO, and atomic scattering factors of their constituent atoms," *Proceedings of the Japan Academy,* 55[2] 43-48 (1979).

31. S. M. Antao, I. Hassan, J. Wang, P. L. Lee, and B. H. Toby, "State-of-the-art high resolution powder X-Ray diffraction (HRPXRD) illustrated with Rietveld structure refinement of quartz, sodalite, tremolite, and meionite," *The Canadian Mineralogist,* 46 1501-09 (2008).

32. C. Bezou, A. Nonat, J. C. Mutin, A. N. Christensen, and M. S. Lehmann, "Investigation of the crystal structure of g $CaSO_4$, $CaSO_4 \cdot 0.5\ H_2O$, and $CaSO_4 \cdot 0.6\ H_2O$ by powder diffraction methods," *Journal of Solid State Chemistry,* 117[1] 165-76 (1995).

33. K. Ojima, Y. Nashihata, and A. Sawada, "Structure of potassium sulfate at temperatures from 296 K down to 15 K," *Acta Crystallographica B,* 51 287-93 (1995).

34. K. Okada and J. Ossaka, "Structure of potassium sodium sulphate and tripotassium sodium disulphate," *Acta Crystallographica B,* 36 919-21 (1980).

35. E. Corazza and C. Sabelli, "The crystal structure of syngenite, $K_2Ca(SO_4)_2.H_2O$," *Zeitschrift für Kristallographie B,* 124 398-408 (1967).

36. D. Speer and E. K. H. Salje, "Phase transitions in langbeinites I: crystal chemistry and structures of K-double sulfates of the langbeinite type M_2^{++} $K_2(SO_4)_3$, M^{++} = Mg, Ni, Co, Zn, Ca," *Physics and Chemistry of Minerals*, 124 398-408 (1986).

37. O. Chaix-Pluchery, J. Pannetier, J. Bouillot, and J. C. Niepce, "Structural prereactional transformations in $Ca(OH)_2$," *Journal of Solid State Chemistry*, 67[2] 225-34 (1987).

38. O. Pritula, L. Smrcok, J. Ivan, and K. Izdinsky, "X-Ray quantitative phase analysis of residues of the reference Portland clinkers," *Ceramics - Silikaty*, 48[1] 34-39 (2004).

39. M. Robledo-Guttierrez, M. T. Blanco-Varela, and P. M. Carmona-Quiroga, "Mineralogical composition of clinker as an indicator of sulfate resistance: a Rietveld XRD/Takashima approach," *Journal of the American Ceramic Society*, 96[11] 3637-42 (2013).

40. P. D. Tennis, S. Bhattacharja, W. A. Klemm, and F. M. Miller, "Assessing the distribution of sulfate in Portland cement and clinker and its influence on expansion in mortar," *Cement, Concrete, and Aggregates*, 21[2] 212-16 (1999).

41. H. W. W. Pollit and A. W. Brown, "The distribution of alkalis in Portland cement clinker,″ in 5th International Symposium on the Chemistry of Cement. Vol. 1. Tokyo, Japan; pp. 322-33 (1968).

42. K. Fukuda and H. Ando, "Determination of the Pcmn/Ibm2 phase boundary at high temperatures in the system $Ca_2Fe_2O_5$–$Ca_2Al_2O_5$," *Journal of American Ceramic Society*, 85[5] 1300-02 (2002).

43. R. D. Shannon, "Revised effective ionic radii and systematic studies of interatomic distances in halides and chalcogenides," *Acta Crystallographica A*, 32 751-67 (1976).

44. D. K. Smith, "Crystallographic changes with the substitution of aluminium for iron in dicalcium ferrite," *Acta Crystallographica*, 15 1146-52 (1962).

45. J. Neubauer, H. J. Kuzel, and R. Sieber, "Rietveld quantitative XRD analysis of Portland cement : II. Quantification of synthetic and technical Portland cement clinker,″ pp. 100-11 in 8th International Conference on Cement Microscopy. Houston, USA; (1996). p 100-11.

46. P. J. Brown, A. G. Fox, E. N. Maslen, M. A. O'Keefe, and B. T. M. Willis, "Intensity of diffracted intensities," *International Tables for Crystallography*, Volume C: mathematical, physical and chemical tables. Section 6.1.1 554-90 (2006).

47. J. Schwartz, "Contribution à l'étude de la phase aluminoferritique des clinkers de ciment Portland," *Revue des Matériaux de Construction*, 669-670 159-72 (1971).

48. K. E. Fletcher, "The composition of the tricalcium aluminate and ferrite phases in Portland cement determined by the use of an electron-probe microanalyser," *Magazine of Concrete Research*, 21[66] 03-14 (1969).

49. M. Regourd, "Cristallochimie des constituants du clinker de ciment Portland," *Revue des Matériaux de Construction*, 695 201-15 (1975).

50. A. Ghose and P. Barnes, "Electron microprobe analysis of Portland cement clinker," *Cement and Concrete Research,* 9 747-55 (1979).

51. C. Hall and K. L. Scrivener, "Oilwell cement clinkers. X-ray Microanalysis and Phase Composition," *Advanced Cement Based Materials,* 7 28-38 (1998).

52. T. B. Bergstrom, C. Hall, and K. L. Scrivener, "Interstitial material in oilwell cements: evidence from X-ray microanalysis," *Advances in Cement Research,* 4[16] 141-47 (1991/92).

53. I. G. Richardson, C. Hall, and G. W. Groves, "TEM study of the composition of the interstitial phase in an oil-well cement clinker," *Advances in Cement Research,* 5[17] 15-21 (1993).

54. M. C. Ball, R. E. Simmons, and I. Sutherland, "Surface composition of anhydrous tricalcium aluminate and calcium aluminoferrite," *Journal of Materials Science,* 22 1975-79 (1987).